Cellular & Molecular Biology Letters

RESEARCH ARTICLE Open Access

Mesenchymal stem cell-secreted KGF ameliorates acute lung injury via the Gab1/ERK/NF-κB signaling axis

Shuning Xin[1], Yan Ding[1], Tong Yu[1], Yunmei Fu[1], Yong Cui[2*] and Hongguang Nie[1*]

*Correspondence: ycui@cmu.edu.cn; hgnie@cmu.edu.cn

[1] Department of Stem Cells and Regenerative Medicine, College of Basic Medical Science, China Medical University, Shenyang 110122, China
[2] Department of Anesthesiology, The First Hospital of China Medical University, Shenyang 110122, China

Abstract

Background: The epithelial sodium channel (ENaC) situated in the apical membrane of alveolar epithelial type 2 (AT2) cells is beneficial to edematous fluid reabsorption in acute lung injury (ALI). Recently, mesenchymal stem cells (MSCs), particularly their secretome, has emerged as a novel approach for treating pulmonary diseases. Among these secreted factors, keratinocyte growth factor (KGF) plays a critical role in mediating alveolar epithelial repair during ALI by enhancing epithelial cell proliferation, restoring epithelial integrity, and alleviating pulmonary edema, making it a promising candidate for therapeutic strategies. This study primarily focused on investigating the impact of KGF secreted from MSC on ALI, and clarifying its specific mechanism in regulating the expression of ENaC.

Methods: Lipopolysaccharide (LPS)-stimulated primary mouse AT2 cells were treated with KGF in vitro, and western blots along with immunofluorescence assays were performed to investigate the regulatory mechanism of KGF on ENaC protein expression. To further confirm the role of mouse bone marrow MSC-derived KGF, co-culture experiments with AT2 cells and either MSC or MSC with KGF knockdown (MSC-siKGF) were conducted. In vivo, an ALI model was established in mice by LPS-induced lung injury. The therapeutic effects of tail vein-injected MSC or MSC-siKGF were assessed using hematoxylin–eosin staining, lung wet/dry weight ratio, and alveolar fluid clearance.

Results: In primary mouse AT2 cells, KGF stimulation effectively restored the reduction of growth factor receptor-bound protein 2-associated binding protein 1 (Gab1) and α/γ-ENaC protein levels induced by LPS. KGF inhibited the activation of the LPS-induced extracellular regulated protein kinases (ERK) and nuclear factor-kappaB (NF-κB) signaling pathway. Treatment with the ERK pathway inhibitor PD98059 reversed the LPS-induced reduction in ENaC protein levels but had no effect on Gab1 levels. In addition, PD98059 suppressed LPS-induced activation of the NF-κB signaling pathway. Further analysis revealed that LPS stimulation weakened the interaction between the NF-κB p65 subunit and inhibitor kappaB (IκB), while KGF enhanced this interaction and inhibited the nuclear translocation of p65. Both KGF and the NF-κB inhibitor QNZ reversed the LPS-induced downregulation of ENaC protein levels and gene expression. Furthermore, both agents effectively restored the functional activity of ENaC channels. Co-culture with MSCs increased Gab1 protein levels,

inhibited ERK/NF-κB signaling activation, and suppressed p65 nuclear translocation in LPS-treated AT2 cells, whereas these effects were attenuated in cells co-cultured with MSC-siKGF. In an ALI mouse model, tail-vein injection of MSCs alleviated lung injury and pulmonary edema, while the therapeutic effects of MSC-siKGF were weaker they were partly restored by the combination of QNZ.

Conclusions: Our study validated that the efficacy of MSCs in the treatment of edematous ALI was significantly associated with KGF, which potentially enhanced the upregulation of ENaC through the Gab1/ERK/NF-κB signaling pathway.

Keywords: Acute lung injury, Epithelial sodium channel, Mesenchymal stem cell, Keratinocyte growth factor, Nuclear factor-kappaB

Introduction

Acute lung injury (ALI)/acute respiratory distress syndrome (ARDS) is a respiratory injury characterized by diffuse alveolar epithelial cell damage that leads to the accumulation of inflammatory fluids and impaired alveolar fluid clearance (AFC), ultimately resulting in high morbidity and mortality [1–4]. The severity of lung epithelial injury, particularly involving alveolar epithelial type 2 (AT2) cells, is a crucial determinant of survival in patients with ALI/ARDS [5]. The epithelial sodium channel (ENaC) located in the apical membrane of AT2 cells, functions as the limiting factor in the process of alveolar epithelial fluid absorption, the dysregulation of which may result in reduced AFC and pulmonary edema [2, 4, 6, 7].

Recently, the paracrine role of mesenchymal stem cells (MSCs) has attracted more and more attention, as it may be the main mechanism of lung injury repair and regeneration [8–14]. Keratinocyte growth factor (KGF), a component of the MSC secretome, has been reported to promote cell survival and proliferation, whereas its detailed role in regulating alveolar epithelial ion transport during ALI/ARDS is still unknown [15–18]. Growth factor receptor binding 2-associated binding protein 1 (Gab1), a highly conserved scaffolding protein, exerts a crucial regulatory role in the KGF signaling pathway, particularly through its interaction with growth factor receptor-bound protein 2 [19, 20]. Furthermore, a recent investigation has demonstrated that the absence of Gab1 in AT2 cells impairs the balance of surfactant proteins, ultimately resulting in lung damage in mice [21]. Therefore, it is important to investigate whether Gab1 plays a significant role in KGF-mediated treatment of ALI. Lipopolysaccharide (LPS) is a well-known inducer of inflammation, which can cause ALI/ARDS in cell/mouse models by activating extracellular regulated protein kinases (ERK) signaling; however, the role of ERK and its downstream nuclear factor-kappaB (NF-κB) signaling is still contradictory in alveolar epithelial cells, both of which are involved in the regulation of ENaC proteins [21–25].

The purpose of this study was to investigate how the paracrine factor KGF secreted by MSCs, affected LPS-induced ALI and associated mechanisms, thereby offering a wide range of clinical applications of MSCs for the treatment of ALI/ARDS.

Methods

Animals and treatment

SPF-grade C57BL/J mice, weighing between 25 and 30 g, or newborn mice (Huafukang, Beijing, China), were utilized for animal experiments. The mice were pretreated with NF-κB specific inhibitor (QNZ, MedChemExpress, Shanghai, China, 1 mg/kg) by

intraperitoneal injection for 0.5 h, followed by LPS (Solarbio, Beijing, China, 5 mg/kg) for 12 h, and MSC/MSC-siKGF (1×10^6 cells) by tail-vein injection for 12 h. The control group was injected with 0.9% NaCl.

Primary mouse AT2 cell and MSC culture

Newborn SPF-grade C57BL/J mice were used to isolate primary AT2 cells. The lung tissue was separated in phosphate-buffered saline (PBS), followed by enzymatic digestion at 37 °C. Then, the collected cells were cultured in Dulbecco's modified Eagle medium (DMEM)/F12 medium (Corning, New York, USA), with the medium changed every 48 h for 3 d before use [22]. Antibodies used in flow cytometry to assess AT2 cell purity included Spc/Pdpn (Santa Cruz, Dallas, USA) and FITC-labeled goat anti-rabbit IgG (ZSGB-bio, Beijing, China). We treated AT2 cells with 100 nM QNZ/10 μM ERK1/2 specific inhibitor (PD98059, Beyotime, Shanghai, China) for 0.5 h, then applied 10 μg/ml LPS for 12 h, followed by KGF (Novoprotein, Suzhou, China, 10 ng/ml) for 12 h.

Following the euthanasia of male C57BL/J mice (25–30 g) by intraperitoneal injection of sodium pentobarbital (100 mg/kg), the femurs were aseptically harvested. The bone marrow cavity was then flushed to collect bone marrow cells, which were subsequently centrifuged and plated into culture dishes containing DMEM/F12 medium [26, 27]. Under optimal culture conditions, nonadherent cells were removed to obtain purified MSCs. To determine the role of KGF in MSC therapy, we transfected 100 nM KGF-siRNA (siKGF, GenePharma, Shanghai, China) for 48 h. MSCs at a density of 1×10^4 cells per well were seeded into the apical compartment of a 6-well Transwell system, while AT2 cells were positioned in the basolateral compartment. AT2 cells treated with 10 μg/mL LPS were co-cultured with MSC/MSC-siKGF for 12 h.

Air–liquid cell culture

Calu-3 cells were seeded at a density of 5×10^6 cells/cm^2 in 24-well Transwell inserts (3413, Corning-Costar, Lowell, USA). The basolateral chamber was filled with DMEM/F12 medium supplemented with 10% fetal bovine serum, 1% penicillin–streptomycin, and 250 nM dexamethasone (D4902, Sigma, St. Louis, USA). The cells were cultured at 37 °C in a humidified incubator with 5% CO_2. After 24 h, unattached cells in the apical chamber were removed, and the culture was switched to an air–liquid interface condition by removing the apical medium, while the basolateral medium was replaced every 48 h. The monolayer integrity was assessed by measuring transepithelial electrical resistance (TEER) using a Millicell ERS-2 V-ohm meter (Millipore, USA), and only monolayers with a stable TEER value exceeding 400 Ω cm^2 were used for subsequent experiments.

Western blot assay

Cellular or tissue proteins were extracted, fractionated by SDS-PAGE gel electrophoresis according to their molecular weights, detected using specific antibodies, and visualized for subsequent expression analysis. The western blot assay utilized primary antibodies that included α-ENaC (1:1500, Invitrogen, Carlsbad, USA); γ-ENaC (1:1500, Abcam, Cambridge, USA); β-actin (1:1500, Proteintech, Chicago, USA); p65, p-p65, inhibitor kappaB (IκB), and p-IκB (1:1000, Abmart, Shanghai, China); ERK1/2 and p-ERK1/2

(1:1000, Cell Signaling, Danvers, USA); and Gab1 (1:500, Affinity, Cincinnati, USA). Horseradish peroxidase-conjugated, goat-anti-rabbit or goat-anti-mouse (1:5000, ZSGB-BIO, Beijing, China) antibodies were used as secondary antibodies at room temperature for 1.5 h. The protein bands were visualized using ECL on a chemiluminescence detection system (Tanon, Shanghai, China), and the intensity of each specific band was quantified with ImageJ.

Immunofluorescence staining

Primary mouse AT2 cells were immobilized using 4% paraformaldehyde at 25 ℃ for 20 min, and nonspecific permeabilization of cell membranes for 15 min with 0.2% Triton X-100. After blocking, the cells were incubated overnight with primary antibody against α/γ-ENaC (1:200), then with anti-rabbit IgG (H + L) highly cross-adsorbed secondary antibody for 2 h. Finally, the cell nuclei were stained with DAPI, and observed under the fluorescence microscope.

Co-immunoprecipitation

The primary mouse AT2 cells were treated with RIPA lysis buffer to extract cell lysates. A specific antibody was used to capture the target protein, forming an antibody–target protein complex, which was then precipitated using protein A/G-beads. During this process, proteins interacting with the target protein were also co-precipitated. Finally, western blot analysis was performed to analyze the interacting proteins.

Electrophoretic mobility shift assay

Nucleoprotein extraction was performed utilizing a dedicated kit sourced from Beyotime (Shanghai, China), with subsequent quantitation of protein concentration. The α-ENaC probe was prepared with the sequence 5′-GGAGAGTCCCC-3′. Next, the nuclear proteins were mixed with DNA probes and allowed to bind under certain conditions. By polyacrylamide gel electrophoresis, protein-bound DNA was separated from unbound DNA. The DNA was then transferred onto a nylon membrane, followed by employing specific detection methods to observe and analyze the positional changes of the DNA probes on the membrane, thereby assessing the binding status of proteins to DNA.

Quantitative real-time polymerase chain reaction

Total RNA was extracted from AT2 cells by Trizol reagent sourced from Invitrogen (Waltham, USA). The PrimeScript RT reagent kit (TaKaRa, Kusatsu, Japan), was utilized to convert the RNA into cDNA according to its guidelines. SYBR Premix Ex Taq II reagent (TaKaRa, Kusatsu, Japan) was used to prepare a reaction system containing the samples and primers, and quantitative real-time polymerase chain reactions (qRT-PCR) were performed on the ABI 7500 qRT-PCR System. The primer pairs included in the experiment were as follows: α-ENaC (forward: 5′-AGG GCT GAG CCT AGA GCT AGA GA-3′; reverse: 5′-TTC CTC CCG GAC TGT TTG AC-3′), β-ENaC (forward: 5′-GGG ACC AAA ACC ACC TTA GCT GCC ATC AC-3′; reverse: 5′-TGC AGT ACC ACA CTA GCA GC-3′), γ-ENaC (forward: 5′-CAG CCG TGA CCC TTC AGT TC-3′; reverse: 5′-CCT TAA TGG TCG GCG CCT GG-3′), and β-actin (forward: 5′-GGC

TGT ATT CCC CTC CAT CG-3′; reverse: 5′-CCA GTT GGT AAC AAT GCC ATG T-3′). The PCR cycling system was set up according to the manufacturer's instructions. The experimental data were analyzed using the $2^{-\Delta\Delta CT}$ relative quantification method.

Hematoxylin–eosin staining

The lung tissues were fixed in 4% paraformaldehyde for 24 h, subsequently dehydrated using a sucrose solution, embedded in paraffin, and then stored in a −80 °C freezer. The paraffin-embedded lung tissues were sectioned using a cryostat, followed by staining with hematoxylin–eosin (HE), and the pathological changes in the lungs were analyzed under an optical microscope. The lung injury score was evaluated on the basis of pulmonary hemorrhage, inflammatory cell infiltration, and pulmonary interstitial edema. According to the severity of injury, scores were assigned as follows: 0 (no apparent lesions), 0.5–1 (mild), 2 (moderate), 3 (severe), and 4 (critical). The ALI score was obtained by summing the scores for each parameter, and the average score for each group was calculated for statistical analysis. All evaluations were performed by an independent observer blinded to the sample identities [28].

Wet/dry weight ratio and lung index measurement

The severity of pulmonary edema was assessed by calculating both the wet/dry (W/D) weight ratio and lung index. Following euthanasia of the mice, lung tissues were promptly isolated and wet weight (g) was determined. Subsequently, these tissues were subjected to drying in an oven maintained at 60 °C for a duration of 48 h. Post-drying, the dry weight (g) of the tissues was measured. Utilizing these values, the W/D weight ratio was computed. In addition, the lung index was derived by dividing the wet weight of the lungs (g) by the total body weight of the mouse (kg).

AFC measurement in vivo

AFC was performed in vivo as previously described [29]. Briefly, after anesthesia with pentobarbital sodium (50 mg/kg) by intraperitoneal injection, the mice were placed supine with their limbs and heads fixed using syringe needles. After exposing and isolating the trachea, a T-connector attached to a mouse respirator was inserted to supply oxygen. The mouse was then positioned laterally, and 200 μl (the volume of injected alveolar fluid, Vi) of 5% (the initial concentration of injected protein, Pi) fatty acid-free bovine serum albumin solution was instilled into the lungs through the T-connector. After 30 min, the respirator was turned off, and a 1 mL syringe connected to the T-connector was used to gently aspirate the alveolar fluid and the protein concentration of the retrieved fluid was measured and recorded as Pf. According to the formula, the volume of alveolar fluid gathered (Vf) can be calculated as $Vf = (Vi \times Pi)/Pf$. Finally, AFC was calculated on the basis of the following formula: $AFC = [(Vi - Vf)/Vi] \times 100$.

Protein interaction prediction using string database

Utilizing the string database (https://string-db.org/), we predicted the downstream signaling pathways of the target protein. The proteins or gene sequences involved in our research were entered to generate a protein–protein interaction network. We then

analyzed each potential interacting protein individually to assess its likelihood of being upstream or downstream of the target protein [30, 31].

Molecular docking analysis

We obtained the molecular structures of the two proteins from the PDB database (https://www.rcsb.org), digitally predicted whether the molecules were likely to bind or not at the zdock website (https://zdock.wenglab.org/), docked the two molecules using PyMol (https://pymol.org/2), and visualized the molecular docking results [32, 33].

Ussing chamber analysis

The Calu-3 monolayers were mounted in Ussing chambers (Physiologic Instruments, San Diego, USA), with the basolateral and apical sides perfused with their respective solutions (composition as previously described) [22]. A continuous flow of 95% O_2/5% CO_2 gas mixture was maintained at 37 °C. To permeabilize the basolateral membrane, 100 μM amphotericin B (Sigma, St. Louis, USA) was added to the basolateral side. After a 10-min equilibration, 100 μM amiloride (Sigma, St. Louis, USA) was applied to the apical side, and the resulting decrease in short-circuit current (Isc) was recorded as the amiloride-sensitive current (ASI), representing ENaC-mediated sodium ion transport. Data were acquired using the Acquire and Analyze 2.3 software.

Measurement of airway surface liquid height

The apical surface of the Calu-3 monolayers was washed three times with PBS, followed by the addition of 1 μL FITC-dextran (Sigma, St. Louis, USA) mixed with 99 μL PBS. The cells were incubated at 37 °C in the dark for 1 h. After removing the apical liquid, the air–liquid interface culture was continued for another 24 h. For analysis, the Transwell membrane was excised and placed in a confocal dish. The airway surface liquid (ASL) was imaged using a laser scanning confocal microscope with *z*-axis 3D scanning (step size: 10 μm). The ASL height was quantified using ImageJ software.

Statistical analysis

The experimental results were presented as the mean ± SE, and assessed the power of sample size firstly to meet $P < 0.05$. Upon successful completion of Levene's test for normality and Shapiro–Wilk's test for heteroscedasticity, we employed one-way analysis of variance (ANOVA) and Bonferroni's test for comparisons across multiple groups.

Results

KGF upregulated Gab1 and ENaC expression

The KGF receptor (KGFR), encoded by the *Fgfr2* gene, is a receptor with high affinity for binding to KGF. Firstly, we utilized the string database to screen Gab1 as a possible candidate molecule in the signaling pathway of KGFR (Fig. 1A) [34]. Molecular docking between Gab1 and KGFR was conducted, which indicated a potential interaction between KGFR and Gab1, with a minimum binding energy of −30.4 kcal/mol (Fig. 1B) [35]. Subsequently, we examined the role of Gab1 in KGF-involved ALI in primary mouse AT2 cells, with a purity up to 90.0% by flow cytometry (Fig. 1C). LPS stimulation significantly downregulated Gab1 protein expression, which could be markedly

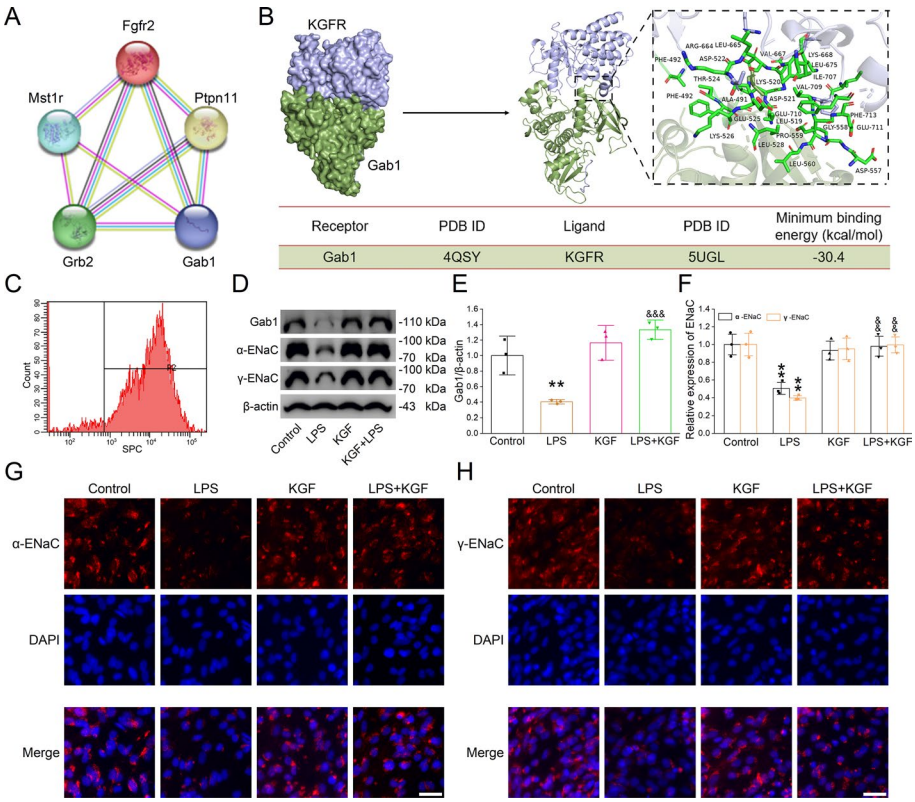

Fig. 1 KGF increased Gab1 and ENaC protein expression in AT2 cells. **A** An analysis of the protein interaction network for the KGFR protein was performed utilizing the string database. **B** The results of molecular docking were visualized, subsequently followed by a detailed magnification of the interacting amino acid pairs. **C** Flow-cytometry results showed 90.0% positivity for the AT2 cell surface marker SPC. **D** Representative graphs showed the effect of LPS or KGF stimulation on α/γ-ENaC and Gab1 protein expression in AT2 cells. **E**, **F** Statistical data were obtained from western blots and quantified through gray analysis. $^{**}P < 0.01$, compared with control group; $^{\&\&}P < 0.01$, $^{\&\&\&}P < 0.001$, compared with LPS group; $n = 3$. Comparison among different groups was analyzed by one-way ANOVA followed by Bonferroni's multiple comparison test. **G**, **H** Immunofluorescence staining of α/γ-ENaC (shown in red) was observed in AT2 cells from different treatment groups. Scale bar: 25 μm

reversed by KGF (Fig. 1D, E). As expected, the key regulator of alveolar fluid absorption, α/γ-ENaC was also significantly enhanced after the administration of KGF in the LPS-induced ALI cell model (Fig. 1F). Notably, the assessment of β-ENaC expression was hindered by the lack of suitable antibodies. Meanwhile, we used immunofluorescence techniques to observe the protein level of α/γ-ENaC in AT2 cells, which was consistent with the above results (Fig. 1G, H).

Gab1 interacted with ERK1/2 protein in AT2 cells

To explore the intermediate signal of how Gab1 regulates ENaC expression, we first screened the possible cross-talk between Gab1 and mitogen activated protein kinase (MAPK) predicted by the string database (Fig. 2A). The interaction between the two proteins was visualized in Fig. 2B, with possible interaction pairs of amino acids enlarged. Further molecular docking of ERK1/2, a family member of the classical MAPK signaling pathway, with Gab1 protein resulted in a minimum binding energy of −15.2 kcal/mol,

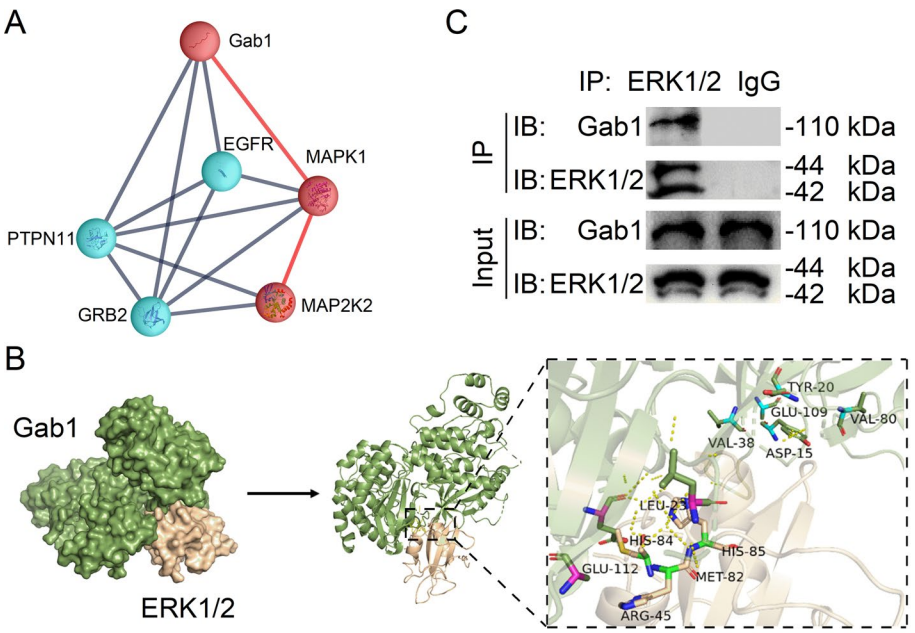

Receptor	PDB ID	Ligand	PDB ID	Minimum binding energy (kcal/mol)
ERK	7AQB	Gab1	4QSY	-15.2

Fig. 2 ERK1/2 interacted with Gab1 protein in AT2 cells. **A** Protein interaction network analysis of the Gab1 protein was conducted using the string database. **B** Visualization of molecular docking results, followed by local magnification of the interacting amino acid pairs. **C** Co-IP assay demonstrated the interaction between Gab1 and ERK1/2

suggesting that the two proteins had the potential to interact with each other, which was validated by co-immunoprecipitation (Co-IP) experiments (Fig. 2C).

Next, the involvement of ERK1/2 in KGF upregulation of ENaC protein was verified. In Fig. 3A, B, LPS could strongly enhance the phosphorylation level of ERK1/2, which was markedly reversed by the administration of KGF. By combining it with the ERK signaling pathway-specific inhibitor PD98059, the inhibitory effect of KGF was not further strengthened. Meanwhile, we found that KGF and PD98059 had similar effects on LPS-reduced α/γ-ENaC protein, whereas only KGF but not PD98059 had a reversible effect on Gab1 expression (Fig. 3C–F), supporting the idea that Gab1 might be one of the upstream molecules of ERK1/2, which could regulate ENaC accordingly.

KGF inhibited NF-κB p65 nuclear translocation through ERK1/2

Our previous studies showed that NF-κB functioned as a downstream pathway associated with the ERK signaling pathway and may participate in the regulation of the ENaC protein [22]. We next investigated the influence of KGF on the NF-κB p65 subunit translocation to the cell nucleus, an essential process for NF-κB phosphorylation activation [15, 22]. The nuclear and total proteins from primary mouse AT2 cells were extracted separately, and the results showed that both KGF and PD98059 significantly inhibited the LPS-enhanced phosphorylation of the NF-κB signaling pathway including p65 and

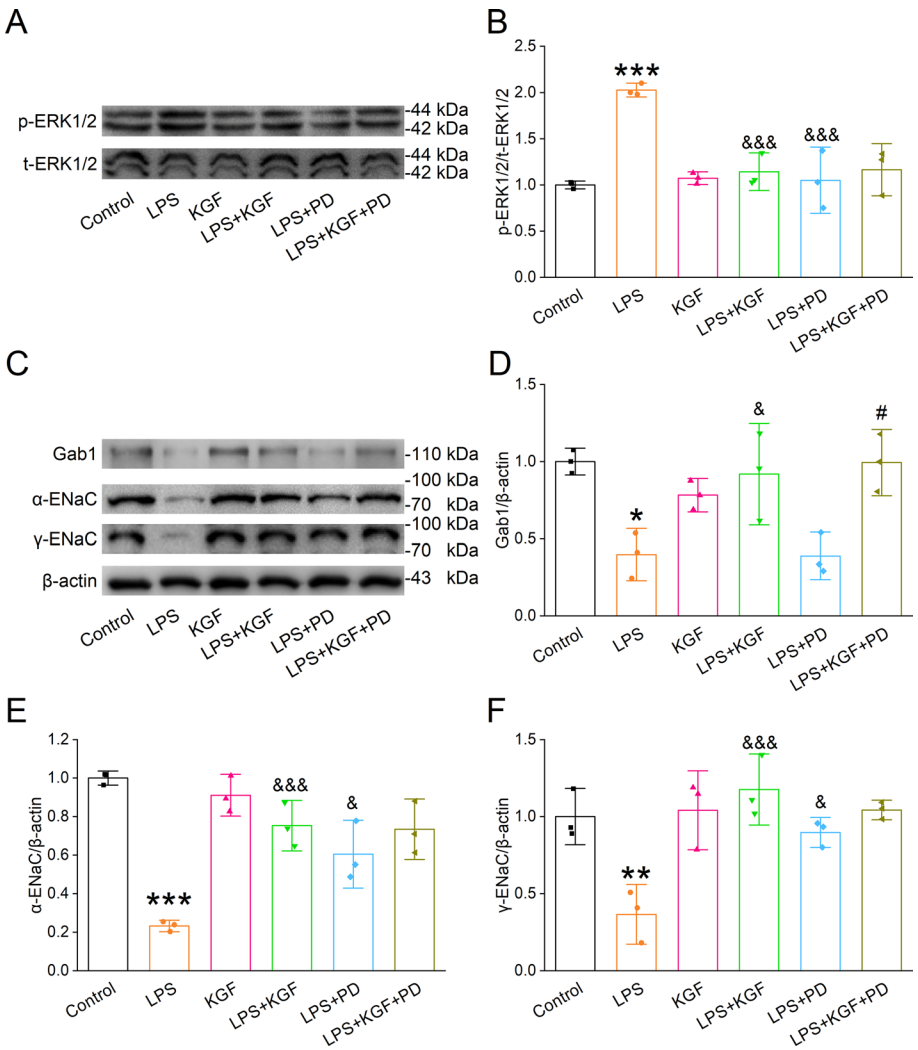

Fig. 3 KGF upregulated ENaC protein expression by inhibiting the ERK phosphorylation. **A**, **B** Representative and statistical data of t-ERK1/2 and p-ERK1/2 after PD98059 or KGF treatment. **C**–**F** Representative western blot and statistical data for Gab1 and α/γ-ENaC. $^{*}P < 0.05$, $^{**}P < 0.01$, $^{***}P < 0.001$, compared with control group; $^{\&}P < 0.05$, $^{\&\&\&}P < 0.001$, compared with LPS group; $^{\#}P < 0.05$, compared with LPS + PD group, $n = 3$. Comparison among different groups was analyzed by one-way ANOVA followed by Bonferroni's multiple comparison test

IκB proteins, as well as the entry of p65 into the nucleus (Fig. 4A–C). The interaction between p65 and the IκB protein was further confirmed by Co-IP experiments (Fig. 4D), consistent with the idea that the binding of IκB concealed the nuclear localization signal of NF-κB, effectively blocking its transport into the nucleus [36, 37]. As shown in Fig. 4E, F, LPS significantly reduced the level of bound IκB (t-IκB/t-p65), which was diminished by the administration of KGF, indicating that KGF inhibited p65 nuclear translocation by enhancing the interaction between p65 and IκB proteins.

Inhibition of NF-κB activation upregulated ENaC expression

To further investigate the impact of activated NF-κB by p65 nuclear translocation on ENaC expression, we employed a NF-κB specific inhibitor (QNZ). As shown in

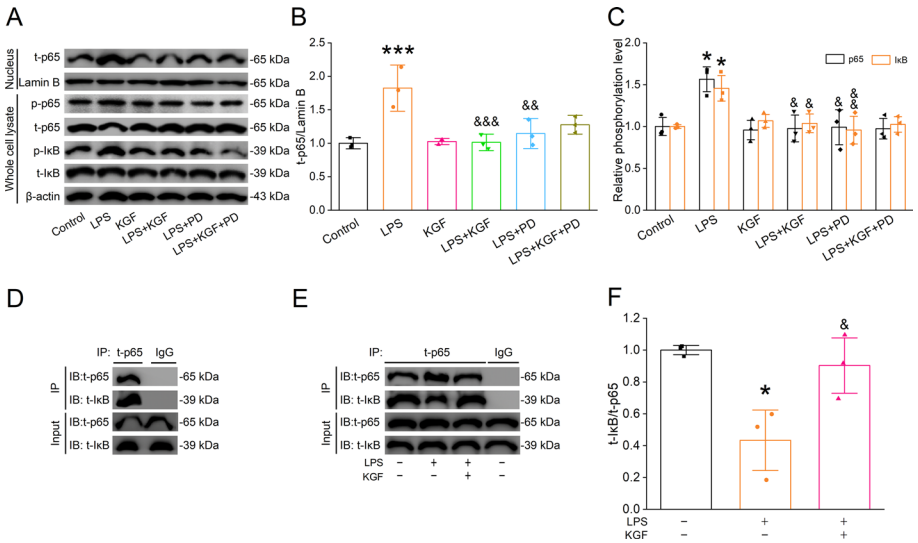

Fig. 4 LPS-induced activation of the NF-κB was suppressed by KGF or PD98059. **A** Illustrative western blot of p-p65/t-p65 and p-IκB/t-IκB in whole cell lysates, along with the nuclear protein p65. **B** Graphical depiction of data derived from western blot assays for nuclear p65 protein. **C** Graphical illustration of data acquired through western blot analysis of whole cell lysates, showing ratios of phosphorylated to total proteins for p65 and IκB. **D** Co-IP assay demonstrates the interaction between t-p65 and t-IκB. **E**, **F** Representative western blot assay and corresponding graphical representation for Co-IP assay. $^{*}P < 0.05$, $^{***}P < 0.001$, compared with control group; $^{\&}P < 0.05$, $^{\&\&}P < 0.01$, $^{\&\&\&}P < 0.001$, compared with LPS group, $n = 3$–5. Comparison among the different groups was analyzed by one-way ANOVA followed by Bonferroni's multiple comparison test

Fig. 5A–E, both KGF and QNZ could significantly inhibit LPS-induced p65 entry into the nucleus and increase α/γ-ENaC protein expression. In the electrophoretic mobility shift assay, nuclear extracts from primary mouse AT2 cells were combined with a biotin-labeled ENaC probe. The observed decrease in the migration rate of the DNA fragment possibly resulted from the direct binding and formation of a complex between ENaC and p65 (Fig. 5F). The β subunit of ENaC alone does not form a functional sodium ion channel, but it significantly enhances channel activity when assembled with the α and γ subunits [38]. Therefore, detecting the expression of β-ENaC is critical for understanding ENaC function. Owing to the lack of a specific antibody, β-ENaC protein levels were not measured in this study. However, we analyzed β-ENaC mRNA expression using specific primers to complement and support the protein-level findings. As expected, at the transcriptional level, either KGF or blocking NF-κB significantly counteracted the LPS-triggered decrease in α/β/γ-ENaC expression (Fig. 5G–I).

KGF rescued ENaC function

Our above data demonstrated that KGF significantly upregulated both ENaC mRNA levels and protein expression. To investigate the regulatory effects of KGF on ENaC function, we first established an air–liquid interface model using Calu-3 cells. As shown in Fig. 6A, cells were seeded in the upper chamber of Transwell inserts, while culture medium was added to the lower chamber to facilitate monolayer formation. The TEER was measured starting from day 4. Compared with day 4, the values were significantly higher on days 8, 10, 12, and 14, and stabilized between days 12 and 16 (Fig. 6B). For subsequent functional assays, cells at day 14 of culture with TEER ≥ 400 Ω cm^2 were

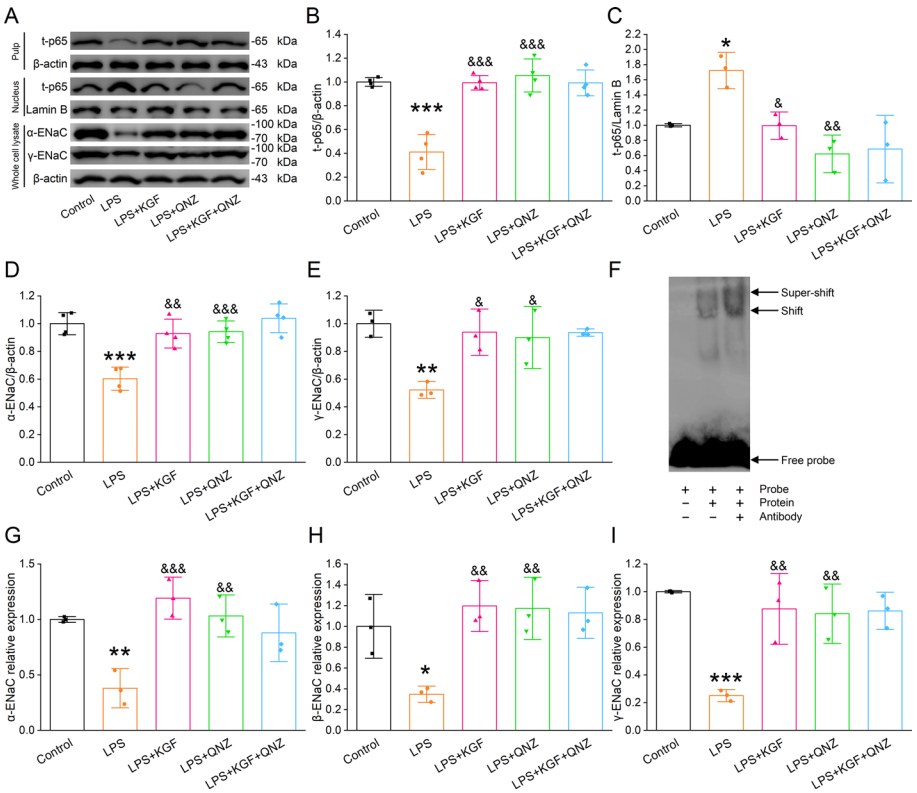

Fig. 5 KGF upregulated ENaC protein expression through inhibiting NF-κB phosphorylation. **A** Illustrative western blot of α/γ-ENaC in whole cell lysates, in addition to the nuclear and pulp protein of p65. **B** Statistical graph of pulp protein p65. **C** Nuclear protein of p65. **D**, **E** Statistical graph of α/γ-ENaC protein expression in whole cell lysates. **F** Electrophoretic mobility shift assay. **G**–**I** The mRNA expression of ENaC by qRT-PCR. $^{*}P < 0.05$, $^{**}P < 0.01$, $^{***}P < 0.001$, compared with control group; $^{\&}P < 0.05$, $^{\&\&}P < 0.01$, $^{\&\&\&}P < 0.001$, compared with LPS group, $n = 3$–4. Comparisons among different groups were analyzed by one-way ANOVA followed by Bonferroni's multiple comparison test

selected. To assess ENaC function, we measured ASI, a key indicator of ENaC activity, using the Ussing chamber system. Once a stable baseline was established, amphotericin B (50 μg/mL) was added to the basolateral side to eliminate transmembrane potential interference. Subsequently, 100 μM amiloride (an ENaC inhibitor) was applied to the apical membrane, and the difference in Isc was used to quantify ASI. The results showed that LPS treatment significantly suppressed ASI, while KGF or QNZ treatment reversed this effect. However, the combination of KGF and QNZ did not exhibit an additive effect (Fig. 6C, D), suggesting that KGF may restore ENaC function by inhibiting the NF-κB signaling pathway. To verify the physiological relevance of ENaC function, we assessed ASL height. Enhanced ENaC activity facilitates sodium absorption, thereby reducing ASL height, whereas impaired ENaC function leads to fluid accumulation. As shown in Fig. 6E, the ASL height in the LPS group was significantly higher than that in the control group, whereas treatment with KGF or QNZ restored ASL height to normal levels, with no further improvement observed in the combination group. The strong consistency between ASL and ASI data indicates that KGF not only upregulates ENaC expression but also directly enhances its functional activity, with NF-κB pathway inhibition playing a pivotal role in this process.

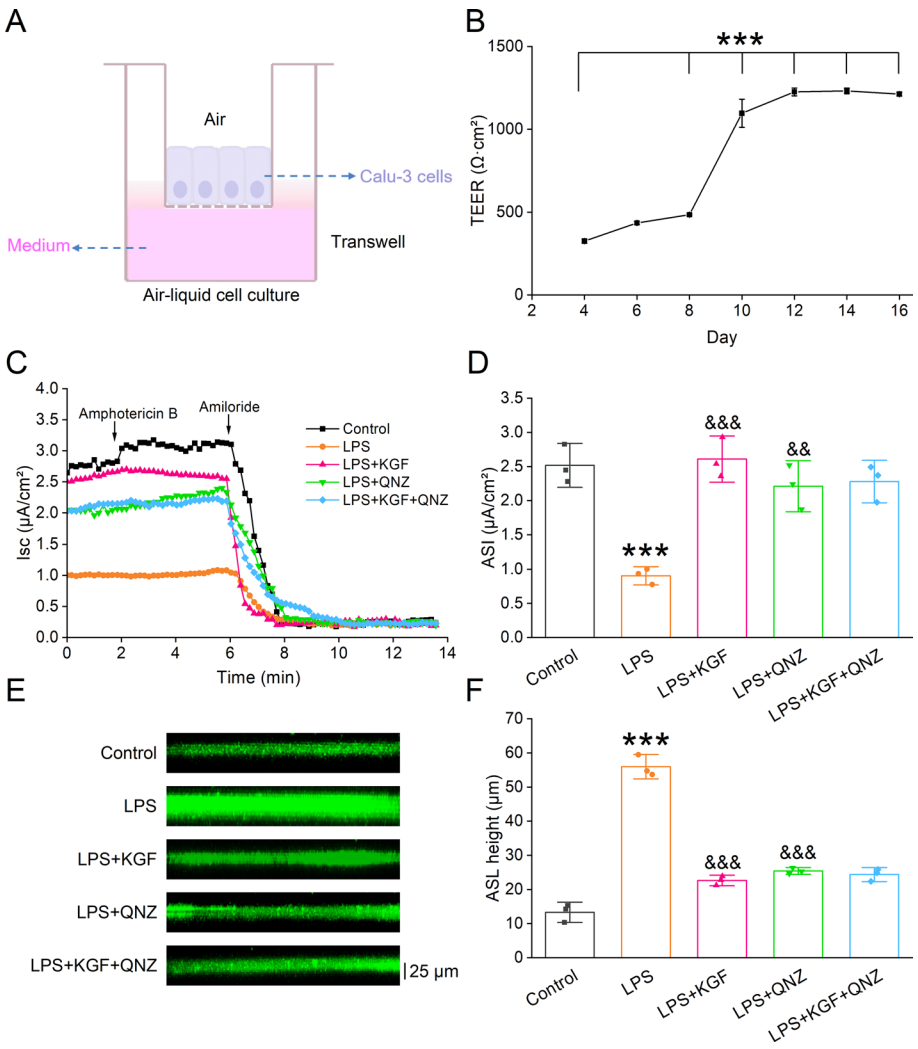

Fig. 6 KGF rescues ENaC function. **A** Schematic representation of Calu-3 cells cultured under air–liquid interface conditions in a Transwell. **B** Change in TEER of the Calu-3 monolayer over the culture period. ***$P < 0.001$, compared with day 4. **C** Isc traces recorded from the Ussing chamber perfusion experiment. **D** Statistical analysis of ASI. **E**, **F** Representative graphs and corresponding graphical representation of ASL height. ***$P < 0.001$, compared with control group; $^{\&\&}P < 0.01$, $^{\&\&\&}P < 0.001$, compared with LPS group, $n = 3$. Comparisons among different groups were analyzed by one-way ANOVA followed by Bonferroni's multiple comparison test

MSC-secreted KGF upregulated ENaC protein expression via the Gab1/ERK/NF-κB signaling axis

We demonstrated that exogenous KGF alleviates ALI by upregulating ENaC protein expression through the Gab1/ERK/NF-κB signaling axis. To further validate whether MSCs exert their therapeutic effect through the secretion of KGF, we co-cultured primary mouse AT2 cells with MSC/MSC-siKGF for further analysis (Fig. 7A). The knockdown efficiency of KGF in MSC was calculated, and 100 nM siKGF was selected for subsequent experiments (Fig. 7B). Western blot analysis of AT2 cell protein extracts revealed that co-culture with MSCs significantly restored α/γ-ENaC protein expression compared with the LPS group. In addition, the restoration of Gab1 protein expression was statistically significant. Notably, compared with the LPS + MSC-Negative Control

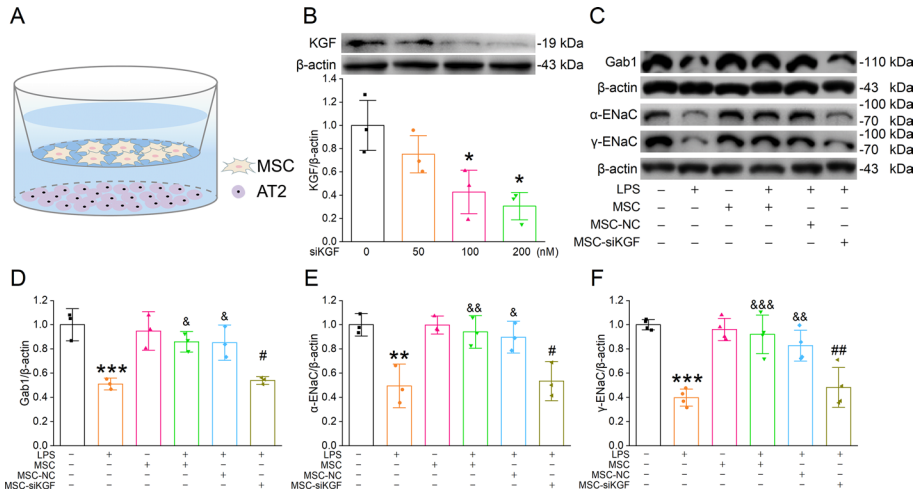

Fig. 7 MSC-secreted KGF regulated Gab1 and ENaC protein level in primary mouse AT2 cells. **A** The co-culture system with AT2 cells and MSCs. **B** KGF knockdown efficiency in primary MSCs. **C**–**F** Representative western blot and corresponding graphical representation for Gab1 and α/γ-ENaC. $^{*}P < 0.05$, $^{**}P < 0.01$, $^{***}P < 0.001$, compared with control group; $^{\&}P < 0.05$, $^{\&\&}P < 0.01$, $^{\&\&\&}P < 0.001$, compared with LPS group; $^{\#}P < 0.05$, $^{\#\#}P < 0.01$, compared with LPS + MSC-NC group, $n = 3$–4. Comparisons among different groups were analyzed by one-way ANOVA followed by Bonferroni's multiple comparison test

(MSC-NC) group, the LPS + MSC-siKGF group exhibited a significant decrease in Gab1 and α/γ-ENaC protein expression. These findings suggest that the protective effect of MSC on α/γ-ENaC and Gab1 expression in AT2 cells is closely associated with its paracrine KGF (Fig. 7C–F).

Further investigation revealed that co-culture with MSCs inhibited the phosphorylation of ERK, p65, and IκB induced by LPS. Compared with the LPS + MSC-NC group, the inhibitory effect on the phosphorylation of ERK, p65, and IκB was weakened in the LPS + MSC-siKGF group. Analysis of nuclear proteins in AT2 cells showed that co-culture with MSCs significantly suppressed LPS-induced nuclear translocation of p65, while MSC-siKGF exhibited a weakened inhibitory effect on p65 nuclear translocation. Therefore, we hypothesize that MSC-derived KGF exerts a similar effect to exogenous KGF (Fig. 8A–E).

MSC-secreted KGF treated ALI/ARDS

To confirm the effect and mechanisms of KGF secreted by MSC in vivo during LPS-triggered ALI, we first examined the histopathological and functional analyses of lung tissues in C57BL/J mice. HE staining (Fig. 9A, B) revealed that, compared with the control group, the LPS-treated group exhibited severe lung injury characterized by alveolar structure disruption, inflammatory cell infiltration, and thickened alveolar septa. These pathological changes were quantified using ALI scores, which demonstrated significant lung injury in the LPS group. Administration of MSC, MSC-siKGF, or QNZ, alleviated LPS-induced lung injury to varying degrees. Specifically, MSC treatment significantly mitigated lung damage, as reflected by improved alveolar architecture and reduced inflammatory infiltration. However, in the LPS + MSC-siKGF group, the therapeutic effects were diminished compared with the LPS + MSC group, indicating that KGF plays a crucial role in MSC-mediated lung protection. Notably, when QNZ was

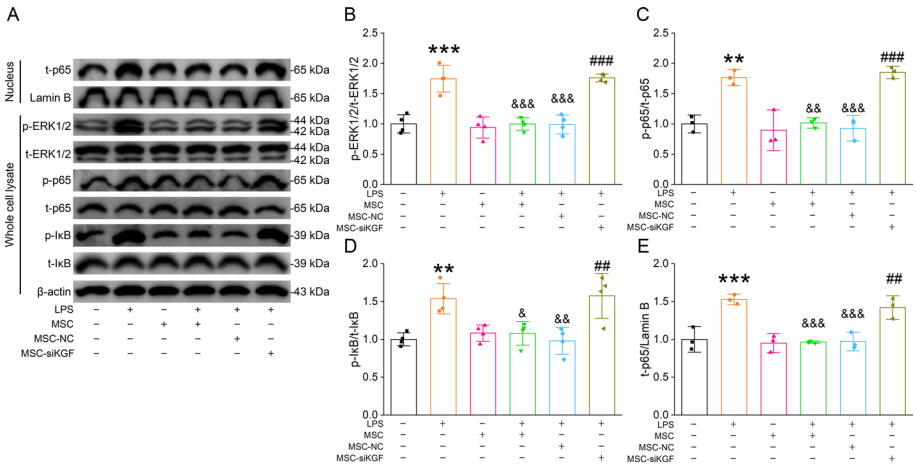

Fig. 8 MSC-secreted KGF inhibited ERK/NF-κB signaling pathway activation. **A** Representative western blot of p-ERK1/2/t-ERK1/2, p-p65/t-p65, and p-IκB/t-IκB in whole cell lysates, as well as the nuclear protein fraction of p65. **B**–**E** Corresponding graphical representation of data obtained from western blot assays for p-ERK1/2/t-ERK1/2, p-p65/t-p65, and p-IκB/t-IκB in whole cell lysates, and nuclear protein p65, respectively. $^{**}P < 0.01$, $^{***}P < 0.001$, compared with control group; $^{\&}P < 0.05$, $^{\&\&}P < 0.01$, $^{\&\&\&}P < 0.001$, compared with LPS group; $^{\#\#}P < 0.01$, $^{\#\#\#}P < 0.001$, compared with LPS + MSC-NC group, $n = 3$–4. Comparisons among different groups were analyzed by one-way ANOVA followed by Bonferroni's multiple comparison test

co-administered with MSC-siKGF (LPS + MSC-siKGF + QNZ group), the lung injury was significantly alleviated compared with the LPS + MSC-siKGF group, suggesting that NF-κB inhibition could partially restore the loss of therapeutic efficacy caused by KGF knockdown. These histological findings were consistent with lung edema-related indices, including AFC, W/D weight ratio, and lung index (Fig. 9C–E). The LPS group exhibited significant pulmonary edema, as indicated by a significantly decreased in AFC and increased the W/D weight ratio and lung index. MSC treatment ameliorated these edema-related indices, whereas this therapeutic effect was impaired in the MSC-siKGF group. Importantly, QNZ treatment in the LPS + MSC-siKGF group restored AFC levels and reduced the W/D weight ratio and lung index, further supporting the role of NF-κB inhibition in compensating for the loss of KGF. In addition, analysis of α/γ-ENaC protein expression in lung tissues provided further evidence of KGF's role in ALI (Fig. 9F–H). The LPS group exhibited downregulated α/γ-ENaC expression, which was significantly restored by MSC treatment. However, KGF knockdown in MSCs reduced α/γ-ENaC expression levels, impairing AFC. Notably, QNZ administration in the MSC-siKGF-treated group restored α/γ-ENaC expression, reinforcing the hypothesis that NF-κB inhibition can mitigate the adverse effects of KGF silencing on lung edema resolution. Collectively, these results demonstrate that MSC-derived KGF is a key factor in mitigating LPS-induced lung injury and edema. However, NF-κB inhibition can partially compensate for the loss of KGF, restoring the therapeutic effects of MSCs even in the absence of KGF expression.

Discussion

Clinical studies in recent years have found that MSC-based cellular therapies can reduce pulmonary edema, relieve inflammation, and thereby alleviate the pathological features of ALI/ARDS [39–43]. Owing to the side effects of vascular obstruction, immune

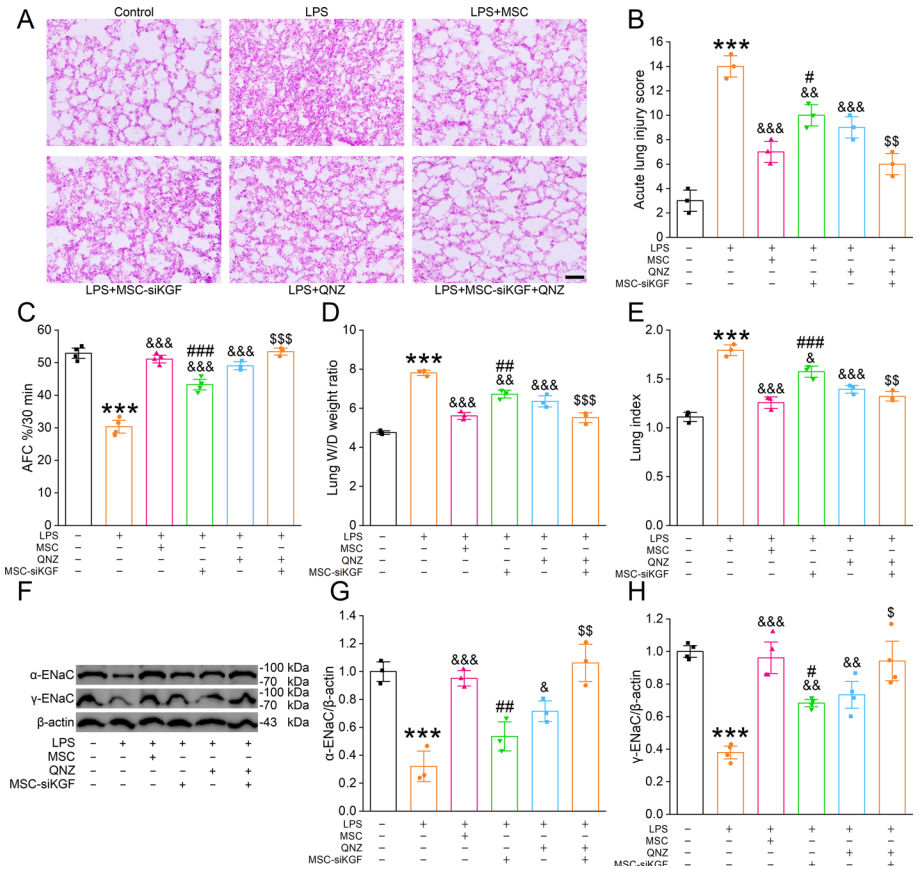

Fig. 9 NF-κB participated in the KGF-mediated improvement of pathological damage and upregulation of ENaC expression in vivo. **A** HE staining of mouse lung tissues. Scale bar: 50 μm. **B** ALI scores. **C** AFC of mice. **D**, **E** The lung W/D weight ratio and lung index. **F**–**H** Representative western blot and corresponding graphical representation for α/γ-ENaC in lung tissues. $^{***}P < 0.001$, compared with control group; $^{\&}P < 0.05$, $^{\&\&}P < 0.01$, $^{\&\&\&}P < 0.001$, compared with LPS group; $^{\#}P < 0.05$, $^{\#\#}P < 0.01$, $^{\#\#\#}P < 0.001$, compared with LPS + MSC group; $^{\$}P < 0.05$, $^{\$\$}P < 0.01$, $^{\$\$\$}P < 0.001$, compared with LPS + MSC-siKGF group, $n = 3$–4. Comparisons among different groups were analyzed by one-way ANOVA followed by Bonferroni's multiple comparison test

rejection, and rapid senescence in MSC therapy, the MSC secretome has attracted researchers' attention, which includes KGF, as one of the most important factors to increase alveolar space and reduce pulmonary edema [15, 44–48]. ENaC serves as the primary factor in establishing an osmotic Na^+ gradient across the lung epithelium, playing a pivotal role in modulating Na^+ transport and efficiently eliminating alveolar edema fluid [2, 6]. Our previous research showed that MSC-conditioned medium including KGF may alleviate pulmonary edema, whereas the relative mechanisms of how MSC-secreted KGF regulated alveolar ion transport was not clear [15].

In the present study, we elucidated the mechanism underlying KGF-mediated ENaC regulation in ALI. Gab1, a scaffold protein linked to the tyrosine kinase KGFR, plays a pivotal role in lung epithelial homeostasis [19], and its disruption is associated with surfactant imbalance and increased susceptibility to lung injury [20]. In our experiment, the enhancement of Gab1 protein expression was first verified after KGF administration in LPS-induced AT2 cell injury models. Using the string database, we forecasted that Gab1 might interact with MAPKs, which included ERK1/2, c-Jun N-terminal kinase,

and p38 [49]. In mouse embryonic fibroblasts and endothelial cells, Gab1 recruitment mediates downstream ERK activation, which is crucial for angiogenesis in vitro [50]. The phosphorylation of ERK declined in lung adenocarcinoma cells after Gab1 knockdown [51]. The fact that blocking ERK1/2 with the specific inhibitor PD98059 had no effect on the LPS-reduced Gab1 protein expression supported the concept that Gab1 was an upstream molecule in the regulation of ERK, although the inverted regulatory role was also reported by epidermal growth factor [50, 52]. The ERK/NF-κB pathway has been reported as a well-established proinflammatory pathway responsible for cytokine production and inflammation initiation [53, 54]. The regulation of NF-κB activity is governed by IκB proteins, which mediate the nuclear–cytoplasmic trafficking and DNA binding of NF-κB [55, 56]. Our data proved that LPS stimulated the phosphorylation of IκB and released the p65 subunit, which could then translocate from the cytoplasm to the nucleus and function as a transcription factor to regulate ENaC gene expression. Furthermore, PD98059 inhibited LPS-induced phosphorylation of NF-κB, consistent with previous studies in hepatocytes [57]. By blocking NF-κB with QNZ, the entry of p65 into the nucleus was inhibited, and the ENaC mRNA and protein expression were subsequently upregulated. Using immunoprecipitation assays with primary mouse AT2 cells, we found that KGF enhanced the protein interaction between p65 and IκB. The finding that KGF acted with a similar mechanism to QNZ, indicated that NF-κB signaling pathway may mediate KGF's involvement in LPS-induced ALI. Meanwhile, the ERK/NF-κB pathway was also found to be involved in regulating ENaC [22]. On the basis of the Ussing chamber perfusion experiment and ASL height measurement, we speculated that KGF may restore ENaC function by inhibiting the NF-κB signaling pathway. Coculture of AT2 cells with MSC-siKGF revealed that KGF knockdown attenuated the role of MSCs in the regulation of the Gab1/ERK/NF-κB/ENaC signaling axis, indicating that the restoration of ENaC protein expression by MSCs was partly mediated by KGF.

At the animal level, LPS-induced mice exhibited prominent characteristics of ALI, such as a decline in AFC, the occurrence of lung edema, and histological findings from HE staining of lung tissues revealing collapsed alveolar structures, thickened alveolar septa, and infiltration of inflammatory cells. The extent of lung injury was significantly reduced after MSC administration, as evidenced by lung tissue injury scores and AFC, whereas the therapeutic effect of MSCs was attenuated after knockdown of KGF. Meanwhile, we found that QNZ could enhance the therapeutic effect of MSC-siKGF, which supported the idea that the therapeutic effect of MSC was at least caused by KGF in its secretome, mediated by the NF-κB signaling pathway. As the key regulator of transepithelial ion transport and a critical factor for edematous fluid reabsorption, the results of α/γ-ENaC protein expression in vivo supported that KGF was the critical ingredient of MSCs in treating edematous ALI (Fig. 10).

Despite the significance of our findings, several limitations should be acknowledged. First, although we identified the Gab1/ERK/NF-κB axis as a key mediator of KGF-induced ENaC regulation, the involvement of additional signaling pathways cannot be ruled out. Future transcriptomic or proteomic studies may provide a broader understanding of the regulatory mechanisms. Second, while molecular docking and Co-IP confirmed interactions between key proteins, further structural studies (e.g., X-ray crystallography or cryo-EM) are needed to elucidate their binding dynamics in greater

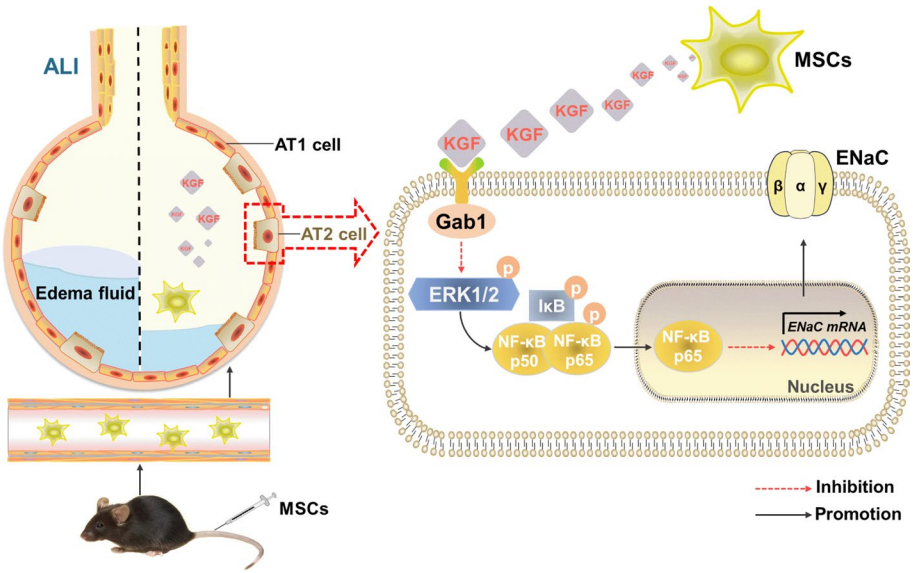

Fig. 10 The schematic diagram depicts the function of MSCs in enhancing the expression of ENaC in ALI induced by LPS. The accumulation of edema fluid in alveoli was a major characteristic in ALI. MSC-secreted KGF upregulates Gab1 protein expression and inhibits the activation of the ERK/NF-κB signaling pathway, thereby upregulating the ENaC protein level in AT2 cells and alleviating LPS-induced pulmonary edema. ALI, acute lung injury; AT1 cell, alveolar type 1 cell; AT2 cell, alveolar type 2 cell; ENaC, epithelial sodium channel; ERK1/2, extracellular regulated protein kinases1/2; Gab1, growth factor receptor binding 2-associated binding protein 1; IκB, inhibitor κB; KGF, keratinocyte growth factor; MSCs, mesenchymal stem cells; NF-κB, nuclear factor-kappa B

detail. Another limitation is that our study utilized a single LPS-induced ALI mouse model, which, while widely used, does not fully replicate the complexity of human ALI/ARDS, which can result from diverse etiologies such as bacterial pneumonia or ventilator-induced lung injury. Future studies should assess the efficacy of MSC-derived KGF in multiple ALI models and evaluate its translational potential in large-animal studies.

Conclusions

Our results indicated that KGF, secreted by MSCs, regulated the expression of ENaC protein through the Gab1/ERK/NF-κB signaling axis, thereby alleviating LPS-induced ALI. We provide evidence that NF-κB inhibition can compensate for the loss of KGF, further supporting the critical role of this pathway in ENaC regulation. These findings offer novel insights into the molecular mechanisms of MSC-mediated lung protection and highlight KGF as a key therapeutic factor. Building on our current findings, future research should focus on strategies to enhance the therapeutic efficacy of MSCs in ALI treatment.

Abbreviations

AFC	Alveolar fluid clearance
ALI	Acute lung injury
ARDS	Acute respiratory distress syndrome
ASI	Amiloride-sensitive current
ASL	Airway surface liquid
AT2	Alveolar epithelial type 2
Co-IP	Co-immunoprecipitation
ENaC	Epithelial sodium channel

ERK	Extracellular regulated protein kinases
Gab1	Growth factor receptor binding 2-associated binding protein
HE	Hematoxylin–eosin
Isc	Short-circuit current
IκB	Inhibitor kappaB
LPS	Lipopolysaccharide
MSC	Mesenchymal stem cell
NF-κB	Nuclear factor-kappa B
qRT-PCR	Quantitative real-time polymerase chain reaction
TEER	Transepithelial electrical resistance
W/D	Wet/dry

Acknowledgements
We thank all the members of our laboratory for their discussions and useful comments.

Author contributions
Shuning Xin: methodology, data curation, software, and writing—original draft preparation. Yan Ding: formal analysis and methodology. Tong Yu: conceptualization and methodology. Yunmei Fu: software and validation. Yong Cui: conceptualization, data curation, and writing—reviewing and editing. Hongguang Nie: conceptualization, funding acquisition, and writing—reviewing and editing.

Funding
This work was supported by grants from the National Natural Science Foundation of China (82170093) to H.N., and Liaoning Province Science and Technology Plan Project (2023JH2/20200072) to Y.D.

Availability of data and materials
All data generated and analyzed to evaluate the conclusions in this study are presented in this article. All primary data can be made available from the corresponding authors upon reasonable request.

Declarations

Ethics approval and consent to participate
All animal studies complied with the ethical guidelines for researchers by the International Council for Laboratory Animal Science (ICLAS) and were approved by the China Medical University Animal Care Committee (permission number: KT2021041; date issued: 23 February 2021).

Consent for publication
Not applicable.

Competing interests
The authors declare no competing interests.

Received: 28 April 2025 Accepted: 17 June 2025
Published online: 10 July 2025

References

1. Fan Y, Moser J, Jongman RM, Borghuis T, Vonk JM, Timens W, et al. Compositional changes of the lung extracellular matrix in acute respiratory distress syndrome. Am J Physiol Cell Physiol. 2025;328:C1279–92. https://doi.org/10.1152/ajpcell.01007.2024.
2. Zhai Y, Yu T, Xin S, Ding Y, Cui Y, Nie H. Network pharmacology-based research into the mechanism of ferulic acid on acute lung injury through enhancing transepithelial sodium transport. J Ethnopharmacol. 2024;330: 118230. https://doi.org/10.1016/j.jep.2024.118230.
3. Qi X, Luo Y, Xiao M, Zhang Q, Luo J, Ma L, et al. Mechanisms of alveolar type 2 epithelial cell death during acute lung injury. Stem Cells. 2023;41:1113–32. https://doi.org/10.1093/stmcls/sxad074.
4. Bos LDJ, Ware LB. Acute respiratory distress syndrome: causes, pathophysiology, and phenotypes. Lancet. 2022;400:1145–56. https://doi.org/10.1016/S0140-6736(22)01485-4.
5. Chen X, Zhang C, Wei T, Chen J, Pan T, Li M, et al. Alpha7nAChR activation in AT2 cells promotes alveolar regeneration through WNT7B signaling in acute lung injury. JCI Insight. 2023;8: e162547. https://doi.org/10.1172/jci.insight.162547.
6. Matalon S, Bartoszewski R, Collawn JF. Role of epithelial sodium channels in the regulation of lung fluid homeostasis. Am J Physiol Lung Cell Mol Physiol. 2015;309:L1229–38. https://doi.org/10.1152/ajplung.00319.2015.
7. Bartoszewski R, Matalon S, Collawn JF. Ion channels of the lung and their role in disease pathogenesis. Am J Physiol Lung Cell Mol Physiol. 2017;313:L859–72. https://doi.org/10.1152/ajplung.00285.2017.
8. Rogulska O, Vavrinova E, Vackova I, Havelkova J, Gotvaldova K, Abaffy P, et al. The role of cytokine licensing in shaping the therapeutic potential of Wharton's jelly MSCs: metabolic shift towards immunomodulation at the expense of differentiation. Stem Cell Res Ther. 2025;16:199. https://doi.org/10.1186/s13287-025-04309-2.
9. Ulpiano C, Salvador W, Franchi-Mendes T, Huang MC, Lin YH, Lin HT, et al. Continuous collection of human mesenchymal-stromal-cell-derived extracellular vesicles from a stirred tank reactor operated under xenogeneic-free conditions for therapeutic applications. Stem Cell Res Ther. 2025;16:210. https://doi.org/10.1186/s13287-025-04341-2.

10. Liu C, Xiao K, Xie L. Advances in the regulation of macrophage polarization by mesenchymal stem cells and implications for ALI/ARDS treatment. Front Immunol. 2022;13: 928134. https://doi.org/10.3389/fimmu.2022.928134.
11. Wu M, Liu J, Zhang S, Jian Y, Guo L, Zhang H, et al. Shh signaling from the injured lung microenvironment drives BMSCs differentiation into alveolar type II cells for acute lung injury treatment in mice. Stem Cells Int. 2024;2024:1823163. https://doi.org/10.1155/2024/1823163.
12. Alvites R, Branquinho M, Sousa AC, Lopes B, Sousa P, Mauricio AC. Mesenchymal stem/stromal cells and their paracrine activity-immunomodulation mechanisms and how to influence the therapeutic potential. Pharmaceutics. 2022;14(2):381. https://doi.org/10.3390/pharmaceutics14020381.
13. Wakayama H, Hashimoto N, Matsushita Y, Matsubara K, Yamamoto N, Hasegawa Y, et al. Factors secreted from dental pulp stem cells show multifaceted benefits for treating acute lung injury in mice. Cytotherapy. 2015;17:1119–29. https://doi.org/10.1016/j.jcyt.2015.04.009.
14. Gazdhar A, Susuri N, Hostettler K, Gugger M, Knudsen L, Roth M, et al. HGF expressing stem cells in usual interstitial pneumonia originate from the bone marrow and are antifibrotic. PLoS ONE. 2013;8: e65453. https://doi.org/10.1371/journal.pone.0065453.
15. Yu T, Cui Y, Xin S, Fu Y, Ding Y, Hao L, et al. Mesenchymal stem cell conditioned medium alleviates acute lung injury through KGF-mediated regulation of epithelial sodium channels. Biomed Pharmacother. 2023;169: 115896. https://doi.org/10.1016/j.biopha.2023.115896.
16. Bartolo I, Reis RL, Marques AP, Cerqueira MT. Keratinocyte growth factor-based strategies for wound re-epithelialization. Tissue Eng Part B Rev. 2022;28:665–76. https://doi.org/10.1089/ten.TEB.2021.0030.
17. Geervliet E, Terstappen L, Bansal R. Hepatocyte survival and proliferation by fibroblast growth factor 7 attenuates liver inflammation, and fibrogenesis during acute liver injury via paracrine mechanisms. Biomed Pharmacother. 2023;167: 115612. https://doi.org/10.1016/j.biopha.2023.115612.
18. Shyamsundar M, McAuley DF, Ingram RJ, Gibson DS, O'Kane D, McKeown ST, et al. Keratinocyte growth factor promotes epithelial survival and resolution in a human model of lung injury. Am J Respir Crit Care Med. 2014;189:1520–9. https://doi.org/10.1164/rccm.201310-1892OC.
19. Zhang YM, Zhang ZQ, Liu YY, Zhou X, Shi XH, Jiang Q, et al. Requirement of Galphai1/3-Gab1 signaling complex for keratinocyte growth factor-induced PI3K-AKT-mTORC1 activation. J Invest Dermatol. 2015;135:181–91. https://doi.org/10.1038/jid.2014.326.
20. Wang K, Qin S, Liang Z, Zhang Y, Xu Y, Chen A, et al. Epithelial disruption of Gab1 perturbs surfactant homeostasis and predisposes mice to lung injuries. Am J Physiol Lung Cell Mol Physiol. 2016;311:L1149–59. https://doi.org/10.1152/ajplung.00107.2016.
21. Sun L, Zhu H, Zhang K. GAB1 alleviates septic lung injury by inhibiting the TLR4/ NF-kappaB pathway. Clin Exp Pharmacol Physiol. 2022;49:94–103. https://doi.org/10.1111/1440-1681.13589.
22. Zhou W, Hou Y, Yu T, Wang T, Ding Y, Nie H. Submersion and hypoxia inhibit alveolar epithelial Na(+) transport through ERK/NF-kappaB signaling pathway. Respir Res. 2023;24:117. https://doi.org/10.1186/s12931-023-02428-z.
23. Chen S, Xie J, Zhao K, Ren L, Deng Y, Xie X, et al. LPS aggravates lung inflammation induced by RSV by promoting the ERK-MMP-12 signaling pathway in mice. Respir Res. 2020;21:193. https://doi.org/10.1186/s12931-020-01453-6.
24. Hong H, Lou S, Zheng F, Gao H, Wang N, Tian S, et al. Hydnocarpin D attenuates lipopolysaccharide-induced acute lung injury via MAPK/NF-kappaB and Keap1/Nrf2/HO-1 pathway. Phytomedicine. 2022;101: 154143. https://doi.org/10.1016/j.phymed.2022.154143.
25. Wang Z, Yang L. Downregulation of ROR2 attenuates LPS-induced A549 cell injury through JNK and ERK signaling pathways. Immun Inflamm Dis. 2023;11: e803. https://doi.org/10.1002/iid3.803.
26. Lu Y, Han Y, Zhou L, Shi G, Bai L, Wang K, et al. A comparative study of mouse bone marrow mesenchymal stem cells isolated using three easy-to-perform approaches. FEBS Open Bio. 2022;12:2154–65. https://doi.org/10.1002/2211-5463.13493.
27. Soleimani M, Nadri S. A protocol for isolation and culture of mesenchymal stem cells from mouse bone marrow. Nat Protoc. 2009;4:102–6. https://doi.org/10.1038/nprot.2008.221.
28. Wu Y, Yu X, Wang Y, Huang Y, Tang J, Gong S, et al. Ruscogenin alleviates LPS-triggered pulmonary endothelial barrier dysfunction through targeting NMMHC IIA to modulate TLR4 signaling. Acta Pharm Sin B. 2022;12:1198–212. https://doi.org/10.1016/j.apsb.2021.09.017.
29. Nie H, Cui Y, Wu S, Ding Y, Li Y. 1,25-Dihydroxyvitamin D enhances alveolar fluid clearance by upregulating the expression of epithelial sodium channels. J Pharm Sci. 2016;105:333–8. https://doi.org/10.1016/j.xphs.2015.11.022.
30. Szklarczyk D, Gable AL, Lyon D, Junge A, Wyder S, Huerta-Cepas J, et al. STRING v11: protein–protein association networks with increased coverage, supporting functional discovery in genome-wide experimental datasets. Nucleic Acids Res. 2019;47:D607–13. https://doi.org/10.1093/nar/gky1131.
31. Szklarczyk D, Kirsch R, Koutrouli M, Nastou K, Mehryary F, Hachilif R, et al. The STRING database in 2023: protein-protein association networks and functional enrichment analyses for any sequenced genome of interest. Nucleic Acids Res. 2023;51:D638–46. https://doi.org/10.1093/nar/gkac1000.
32. Pierce BG, Wiehe K, Hwang H, Kim BH, Vreven T, Weng Z. ZDOCK server: interactive docking prediction of protein-protein complexes and symmetric multimers. Bioinformatics. 2014;30:1771–3. https://doi.org/10.1093/bioinformatics/btu097.
33. Zhang Y, Wang X, Zhang Z, Huang Y, Kihara D. Assessment of protein-protein docking models using deep learning. Methods Mol Biol. 2024;2780:149–62. https://doi.org/10.1007/978-1-0716-3985-6_10.
34. Yoodee S, Peerapen P, Plumworasawat S, Malaitad T, Thongboonkerd V. Identification and characterization of ARID1A-interacting proteins in renal tubular cells and their molecular regulation of angiogenesis. J Transl Med. 2023;21:862. https://doi.org/10.1186/s12967-023-04750-y.
35. Ji L, Song T, Ge C, Wu Q, Ma L, Chen X, et al. Identification of bioactive compounds and potential mechanisms of scutellariae radix-coptidis rhizoma in the treatment of atherosclerosis by integrating network pharmacology and experimental validation. Biomed Pharmacother. 2023;165: 115210. https://doi.org/10.1016/j.biopha.2023.115210.

36. Magnani M, Crinelli R, Bianchi M, Antonelli A. The ubiquitin-dependent proteolytic system and other potential targets for the modulation of nuclear factor-kB (NF-kB). Curr Drug Targets. 2000;1:387–99. https://doi.org/10.2174/1389450003349056.
37. Antonia RJ, Hagan RS, Baldwin AS. Expanding the view of IKK: new substrates and new biology. Trends Cell Biol. 2021;31:166–78. https://doi.org/10.1016/j.tcb.2020.12.003.
38. Noreng S, Bharadwaj A, Posert R, Yoshioka C, Baconguis I. Structure of the human epithelial sodium channel by cryo-electron microscopy. Elife. 2018;7(7): e39340. https://doi.org/10.7554/eLife.39340.
39. Chen X, Wu S, Tang L, Ma L, Wang F, Feng H, et al. Mesenchymal stem cells overexpressing heme oxygenase-1 ameliorate lipopolysaccharide-induced acute lung injury in rats. J Cell Physiol. 2019;234:7301–19. https://doi.org/10.1002/jcp.27488.
40. Wu B, Xu MM, Fan C, Feng CL, Lu QK, Lu HM, et al. STING inhibitor ameliorates LPS-induced ALI by preventing vascular endothelial cells-mediated immune cells chemotaxis and adhesion. Acta Pharmacol Sin. 2022;43:2055–66. https://doi.org/10.1038/s41401-021-00813-2.
41. Fernandez-Francos S, Eiro N, Gonzalez-Galiano N, Vizoso FJ. Mesenchymal stem cell-based therapy as an alternative to the treatment of acute respiratory distress syndrome: current evidence and future perspectives. Int J Mol Sci. 2021;22(15):7850. https://doi.org/10.3390/ijms22157850.
42. Shao F, Liu R, Tan X, Zhang Q, Ye L, Yan B, et al. MSC transplantation attenuates inflammation, prevents endothelial damage and enhances the angiogenic potency of endogenous MSCs in a model of pulmonary arterial hypertension. J Inflamm Res. 2022;15:2087–101. https://doi.org/10.2147/JIR.S355479.
43. Hu X, Liu L, Wang Y, Yu Y, Li Z, Liu Y, et al. Human umbilical cord-derived mesenchymal stem cells alleviate acute lung injury caused by severe burn via secreting TSG-6 and inhibiting inflammatory response. Stem Cells Int. 2022;2022:8661689. https://doi.org/10.1155/2022/8661689.
44. Lin H, Chen H, Zhao X, Chen Z, Zhang P, Tian Y, et al. Advances in mesenchymal stem cell conditioned medium-mediated periodontal tissue regeneration. J Transl Med. 2021;19:456. https://doi.org/10.1186/s12967-021-03125-5.
45. Liu Y, Chen J, Liang H, Cai Y, Li X, Yan L, et al. Human umbilical cord-derived mesenchymal stem cells not only ameliorate blood glucose but also protect vascular endothelium from diabetic damage through a paracrine mechanism mediated by MAPK/ERK signaling. Stem Cell Res Ther. 2022;13:258. https://doi.org/10.1186/s13287-022-02927-8.
46. Tian Y, Deng Q, Yang X, Wang C, Le Minh V, Ji R, et al. ISX-9 promotes KGF secretion from MSCs to alleviate ALI through NGFR-ERK-TAU-beta-catenin signaling axis. Stem Cells Transl Med. 2024;13:255–67. https://doi.org/10.1093/stcltm/szad085.
47. Wang H, Zheng R, Chen Q, Shao J, Yu J, Hu S. Mesenchymal stem cells microvesicles stabilize endothelial barrier function partly mediated by hepatocyte growth factor (HGF). Stem Cell Res Ther. 2017;8:211. https://doi.org/10.1186/s13287-017-0662-7.
48. McAuley DF, Curley GF, Hamid UI, Laffey JG, Abbott J, McKenna DH, et al. Clinical grade allogeneic human mesenchymal stem cells restore alveolar fluid clearance in human lungs rejected for transplantation. Am J Physiol Lung Cell Mol Physiol. 2014;306:L809–15. https://doi.org/10.1152/ajplung.00358.2013.
49. Anerillas C, Abdelmohsen K, Gorospe M. Regulation of senescence traits by MAPKs. Geroscience. 2020;42:397–408. https://doi.org/10.1007/s11357-020-00183-3.
50. Li Y, Chai JL, Shi X, Feng Y, Li JJ, Zhou LN, et al. Galphai1/3 mediate Netrin-1-CD146-activated signaling and angiogenesis. Theranostics. 2023;13:2319–36. https://doi.org/10.7150/thno.80749.
51. Song X, Fan PD, Bantikassegn A, Guha U, Threadgill DW, Varmus H, et al. ERBB3-independent activation of the PI3K pathway in EGFR-mutant lung adenocarcinomas. Cancer Res. 2015;75:1035–45. https://doi.org/10.1158/0008-5472.CAN-13-1625.
52. Yu CF, Liu ZX, Cantley LG. ERK negatively regulates the epidermal growth factor-mediated interaction of Gab1 and the phosphatidylinositol 3-kinase. J Biol Chem. 2002;277:19382–8. https://doi.org/10.1074/jbc.M200732200.
53. Zhi L, Ang AD, Zhang H, Moore PK, Bhatia M. Hydrogen sulfide induces the synthesis of proinflammatory cytokines in human monocyte cell line U937 via the ERK-NF-kappaB pathway. J Leukoc Biol. 2007;81:1322–32. https://doi.org/10.1189/jlb.1006599.
54. Zhang H, Wang ZW, Wu HB, Li Z, Li LC, Hu XP, et al. Transforming growth factor-beta1 induces matrix metalloproteinase-9 expression in rat vascular smooth muscle cells via ROS-dependent ERK-NF-kappaB pathways. Mol Cell Biochem. 2013;375:11–21. https://doi.org/10.1007/s11010-012-1512-7.
55. Valovka T, Hottiger MO. p65 controls NF-kappaB activity by regulating cellular localization of IkappaBbeta. Biochem J. 2011;434:253–63. https://doi.org/10.1042/BJ20101220.
56. Hu X, Zhang H, Zhuang L, Jin G, Yang Q, Li M, et al. Ubiquitin-fold modifier-1 participates in the diabetic inflammatory response by regulating NF-kappaB p65 nuclear translocation and the ubiquitination and degradation of ikappaBalpha. Drug Des Devel Ther. 2020;14:795–810. https://doi.org/10.2147/DDDT.S238695.
57. Ghosh J, Das J, Manna P, Sil PC. Hepatotoxicity of di-(2-ethylhexyl)phthalate is attributed to calcium aggravation, ROS-mediated mitochondrial depolarization, and ERK/NF-kappaB pathway activation. Free Radic Biol Med. 2010;49:1779–91. https://doi.org/10.1016/j.freeradbiomed.2010.09.011.

Publisher's Note